

Dynamics of Rapidly Rotating Bose-Einstein Quantum Droplets

Szu-Cheng Cheng,¹ Yu-Wen Wang,² and Wen-Hsuan Kuan^{2,*}

¹*Department of Physics, Chinese Culture University, Yang-Ming-Shan, Taipei 11114, Taiwan.*

²*Department of Applied Physics and Chemistry, University of Taipei, Taipei 10048, Taiwan.*

(Dated: May 3, 2023)

This work theoretically investigates the dynamics of trapped rapidly rotating Bose-Einstein droplets governed by the modified Gross-Pitaevskii equation with the inclusion of the Lee-Huang-Yang nonlinear interaction. Mimicking the quantum Hall systems, the stationary properties of droplets are obtained by minimizing the energy functional established based on the Laughlin-like wavefunction including Landau-Level mixing. By tuning the particle-particle interaction and rotation speed, the preference for the formation of the center-of-mass state, vortex state, and off-centered vortex state can be distinguished in the phase diagram. Under fast rotations, the highly-spiral phase portraits reveal that the emergence of huge vortices with high angular momentum would stabilize the droplets against centrifugal depletion. By solving Euler-Lagrange equations, the periodicity and stability of each phase's breathing and trajectory during long-term evolution are analyzed. The supposition of gauge-induced azimuthal and linear flows results in the generation of nonuniform persistent currents of multiply quantized circulations and reveals the signature of partially coherent superfluids with the nonlinear-modulated self-bound effect.

I. INTRODUCTION

Using laser cooling and trapping techniques, experimentalists can create atomic quantum gases at extremely low temperatures. Today, we know that the phase transition for indistinguishable particles is purely the consequence of quantum statistical effects. According to the Bose-Einstein statistics, the grand canonical ensemble theory reveals the emergence of the quantum phase transition as the chemical potential approaches zero, and by calculating the phase space filling one can further define the critical temperature. Having the same quantum configuration and sharing almost the same energy state, the macroscopic collection of cold atoms with a nonzero off-diagonal long-range order forms the Bose-Einstein condensates (BECs) [1–3]. With the mean-field (MF) approximation, the dynamics of the BECs with weak interatomic interactions can be adequately described through the application of the Gross-Pitaevskii equation (GPE). Near the Feshbach resonance, where the elastic scattering can be dramatically altered by an external field [4–6], a quasibound molecule can tunnel across a potential energy barrier and resonantly couple with the free states of the colliding atoms. Therefore, the possibility of tuning the magnitude and sign of the scattering length with external magnetic fields provides new perspectives on the manipulation of BECs [1, 7, 8].

Concerning the two-body interactions between a monatomic ensemble, an equilibrium between attractive interatomic forces and short-range repulsion due to the van der Waals forces will lead to the formation of a liquid in the cooling processes instead of a gas. Because of the high density and incompressibility, the attempts by usual liquids to enter the quantum regime are prohibited. However, with the inclusion of the Lee-Huang-Yang (LHY) correction to the ground state energy of a homogeneous weakly repulsive Bose gas [9], a new type of quantum liquid which emerges in the ultracold and extremely dilute atomic systems, violating the van der Waals model, has recently been observed in the two-component Bose mixtures [10–12] and single-component dipolar condensates [13–16]. Above the particle number threshold, the gas-to-liquid phase transition takes place when the instabilities arising from attractive mean-field interaction $\propto n^2$ are compensated for by the high-order quantum many-body effects, $\propto n^{5/2}$ [17]. By tuning the interatomic interactions, the realization of the dilute and weakly interacting self-bound liquid droplets provides direct evidence of the beyond MF effects [18].

Being a paradigm for quantum liquids, the superior coherence of the Bose superfluids is demonstrated by calculating the one-body density matrix and the correlation function between any two particles. To describe them, the introduction of the order parameter along with the low-lying elementary excitations obtained from the solutions to the Bogoliubov equations manifest the essence of the quantum fluctuations in the quantum phase transitions. For spinless atomic gases, the gradient of the phase of the condensate wavefunction defines the superfluid velocity, which is irrotational unless there is a singularity embedded in the phase of the order parameter such that the Onsager-Feynmann quantization condition is satisfied. Through laser-stirred phase imprinting, the generation of vortex cores [19, 20], vortex rings [21, 22], and even vortex lattices [23, 24] in rapidly rotating dilute-gas BECs has been experimentally

* wenhsuan.kuan@gmail.com

realized. In tightly trapped BECs, the formation of multiple quantized vortices and long-lived vortex aggregations has also been observed [25, 26], showing the crucial influence of the Coriolis forces in the rotating systems.

Contrary to the gaseous BECs, the quantum droplets with embedded vorticity are metastable in the single-component dipolar condensate [27]. However, it was reported that stable solutions can be theoretically found for the 2D quantum droplets (QDs) with hidden and explicit vorticity [28] and the 3D binary condensates with contact and LHY-amended interactions [29]. It has also been experimentally shown that the application of optical lattices helps to stabilize zero-vorticity and vortical solitons and even multipeak modes for 1D solitons [30]. These studies show that since the nonlinear competitions depict the domain boundaries for the vortex rings of a spinning droplet, the atom number for systems where the finite size effects are relevant is critical to the formation of the low-energy modes. The presence of the lattice potential restricts the axisymmetric solutions and breaks the spatial uniformity, isotropy, and the conservation of the linear and angular momenta.

Just as the neutral superfluids can be induced by rotation, charged superfluids can be initiated by a magnetic field. In 2D electron systems, the observation of quantum Hall (QH) effects reveals remarkable macroscopic quantum phenomena related to topological investigations. For example, vortices, the known stable topological solitons in quantum field theory, are realized as coherent states describing collective excitations of the basic field. The objective of this work is to investigate the dynamics of 2D rapidly rotating quantum droplets within quadratic plus quartic trapping potentials. Since the radial confinements are reduced by the centrifugal potential, the Coriolis force experienced by the droplets in the rotating frame appears as equivalent to the Lorentz force on a charged particle. As the analogy between the QH effects and the rapidly rotating BECs has been precisely recognized, it would be interesting to see whether the artificial Lorentz forces can also be engineered for the new type of quantum liquid such that the generation of exotic phases of multiple topological charges and the Landau-level mixing (LLM) effects can be observed, and the stability of the quantum states can be explored in this system. This would make it possible to simulate the QH-type effects in a controlled manner with the nonuniform quantum liquids. The combined effect of interactions and quantum statistics eventually determines the features of the many-body ground state. Such rotating systems, therefore, allow us to study artificial orbital magnetism in quantum liquids.

II. THEORETICAL MODEL

To form a 2D quantum droplet in the system of dilute Bose-Bose mixtures with densities n_\uparrow and n_\downarrow , a weakly attractive interaction for the interspecies and a weakly repulsive interaction for the intraspecies are required. It has been proven that by writing the short-range interaction in terms of the coupling constant $\tilde{g}_{\sigma\sigma'}$ and the scattering length $a_{\sigma\sigma'}$ via $\tilde{g}_{\sigma\sigma'} = (4\pi\hbar^2/M)/\ln(4e^{-2\gamma}/a_{\sigma\sigma'}^2\Delta)$, where γ is the Euler constant and Δ is chosen such that $\tilde{g}_{\uparrow\downarrow}^2 = \tilde{g}_{\uparrow\uparrow}\tilde{g}_{\downarrow\downarrow}$, the weakly interacting regime beyond the MF approximation can be theoretically approached [31, 32] using the scattering t matrix [33]. For the symmetric case $a_{\uparrow\uparrow} = a_{\downarrow\downarrow} = a$ and $n_\uparrow = n_\downarrow = n$, the calculation of the energy density of a uniform liquid within the assumption of a macroscopic condensate population gives $E_{2D} = (4\kappa\hbar^2n^2/M)\ln(e^{2r+1/2}\kappa aa_{\uparrow\downarrow}n)$, in which $\kappa = 2\pi/\ln(a_{\uparrow\downarrow}/a)$. It can be further simplified to $E_{2D} = (2\kappa^2\hbar^2n^2/\pi M)\ln(n/en_0)$ by introducing the equilibrium density $n_0 = e^{-2r-3/2}/\kappa aa_{\uparrow\downarrow}$ for each component. As a result, after the energy density E_{2D} including all allowed scattering paths is calculated, the liquid phase properties in free space can be obtained by minimizing the grand potential density at zero pressure.

With the inclusion of a modified LHY potential, the time-dependent GPE for a quartic anharmonically-trapped rotating QD viewed in the rotating frame of reference can be written as

$$i\hbar\frac{\partial\Psi}{\partial t} = \frac{1}{2M}(-i\hbar\vec{\nabla} - M\Omega\hat{z} \times \vec{r})^2\Psi + \left[\frac{1}{2}M(\omega_0^2 - \Omega^2)r^2 + \frac{1}{4}\lambda'r^4\right]\Psi + \frac{4\sigma\kappa\hbar^2n_0}{M}|\Psi|^2\ln(|\Psi|^2/n_0)\Psi \quad (1)$$

in which σ is a tunable constant for the nonlinear coefficient adjustment with the three-dimensional experimental data in a quasi-2D system. The first term of Eq. (1) precisely shows that the rotating droplet moves as a charge $-e$ in the xy plane subjected to a synthesized magnetic field $B\hat{z}$ with a vector potential $(e/c)\vec{A} = M\Omega\hat{z} \times \vec{r}$, giving the cyclotron frequency $\Omega = eB/2Mc$. Setting the effective magnetic length equal to unity and applying the Rodrigues definition of the associated Laguerre polynomial

$$L_n^k(t) = \frac{1}{n!}e^{t-t^k}\frac{d^n}{dt^n}(e^{-t}t^{n+k}), \quad (2)$$

the eigenfunctions of the free part of the Hamiltonian

$$\chi_{n,m}(\vec{r}) = \frac{(-1)^n}{\sqrt{2\pi}} \sqrt{\frac{n!}{2^m(m+n)!}} r^m e^{-r^2/4} e^{-im\phi} L_n^m\left(\frac{r^2}{2}\right), \quad (3)$$

can be derived, where integers n and m correspond to the Landau level index and the degenerate states within a Landau level, respectively. For low-dimensional uniform liquids, it is found that the typical length scale on which Ψ changes is in order of the healing length, and the surface tension is crucial to the finite size effects on the droplet's energy and surface mode spectrum. To generalize the investigation of nonuniform liquids, a strong confinement is imposed with the sum of quadratic and quartic components, which manages to compensate for the centrifugal repulsion and stabilize the deformed droplet under fast rotations. Moreover, as the centrifugal potential $-M\Omega^2 r^2/2$ becomes influential at rapid rotations, the combined trapping potential leads to an effective Mexican hat trap. The atomic liquid becomes similar to the complex Schrödinger field interacting with the electromagnetic field in the Higgs-type potential, where the magnetic flux is squeezed into quantized vortices as is well-known in superconductors. This similarity may thus bring the topological relevance between vortex solitons and rotating droplets.

While the presence of the attractive inter-particle interactions will mix different (n, m) states, the lowest Landau level approach would be insufficient to describe the rotating droplets, especially for the strongly confined atoms since the density will not be thinned out in the xy plane as was observed in the vortex lattices. Mimicking the QH systems, we can obtain the stationary properties of the droplet matter waves governed by Eq. (1) by minimizing the energy functional $E[\Psi, \Psi^*]$ constructed using the Laughlin-like wavefunctions with LLM:

$$\Psi = C_m (\mathcal{Z} - \mathcal{Z}_0)^m \exp \left[-\frac{(\vec{r} - \vec{R})^2}{4\rho^2} - \frac{i}{2l_z^2} \hat{z} \cdot (\vec{r} \times \vec{R}) \right] \exp \left[i\frac{\alpha}{4} (\vec{r} - \vec{R})^2 \right] \exp \left[i\frac{\vec{p}}{2\hbar} \cdot (\vec{r} - \vec{R}) \right], \quad (4)$$

where, specified by the unit length l_z , ρ sketches the width of the wavepacket and $\vec{r} = x\hat{x} + y\hat{y}$ is the position of the particle in the droplet, whereas $\vec{R} = X_0\hat{x} + Y_0\hat{y}$ denotes the center-of-mass (CM) position, and α and \vec{p} are the conjugate curvature coefficient and momentum representative of the inherent MF expansion and the relative repulsion of the wavepacket, respectively. The inclusion of an additional phase arising from rotation ensures the Gauge invariance. In the absence of the dissipation due to three-body collisions, the particle number is conserved, and we obtain the wavefunction coefficient $C_m = \sqrt{N2^{m+1}/\pi m!}/\rho^{m+1}$. For convenience, we map the system onto a 2D complex plane by introducing the dimensionless complex coordinates $\mathcal{Z}_0 = \frac{1}{2}(X_0 + iY_0)$, $\mathcal{Z} = \frac{1}{2}(x + iy)$, and momentum $\mathcal{P} = \frac{1}{2}(p_x + ip_y)$. In this manner, the wavefunction can be reconstructed as

$$\begin{aligned} \Psi = C_m (\mathcal{Z} - \mathcal{Z}_0)^m \exp \left[-\frac{1}{\rho^2} |\mathcal{Z} - \mathcal{Z}_0|^2 \right] \exp [\mathcal{Z}^* \mathcal{Z}_0 - \mathcal{Z} \mathcal{Z}_0^*] \exp [i\alpha |\mathcal{Z} - \mathcal{Z}_0|^2] \\ \times \exp [i\mathcal{P}^* (\mathcal{Z} - \mathcal{Z}_0) + i\mathcal{P} (\mathcal{Z}^* - \mathcal{Z}_0^*)]. \end{aligned} \quad (5)$$

To investigate the QD's dynamics and the configuration stability, we employ Hamilton's principle of least action

$$\delta S[\Psi^*, \Psi] = \int dt \int d\vec{r} \delta \mathcal{L}(\Psi, \Psi^*, \dots) = 0, \quad (6)$$

based on the stationary condition for any Lagrangian density \mathcal{L} constructed with the wavefunction, its complex conjugate, and their derivatives given by

$$\mathcal{L} = \frac{i\hbar}{2} \left(\Psi^* \frac{\partial \Psi}{\partial t} - \Psi \frac{\partial \Psi^*}{\partial t} \right) - \Psi^* H \Psi. \quad (7)$$

Within the dimensionless formulation, the spatial integration of the Lagrangian density involving the time derivative terms gives

$$\int \frac{i}{2} \left(\Psi^* \frac{\partial \Psi}{\partial t} - \Psi \frac{\partial \Psi^*}{\partial t} \right) d\vec{r} = -iN(\mathcal{Z}^* \dot{\mathcal{Z}}_0 - \mathcal{Z} \dot{\mathcal{Z}}_0^*) - \frac{N}{2} (m+1) \dot{\alpha} \rho^2 + N(\mathcal{P}^* \dot{\mathcal{Z}}_0 + \mathcal{P} \dot{\mathcal{Z}}_0^*). \quad (8)$$

Based on the transformation relations $\partial/\partial \mathcal{Z} = \partial/\partial x - i\partial/\partial y$ and $\partial/\partial \mathcal{Z}^* = \partial/\partial x + i\partial/\partial y$, we define the complex creation and annihilation operators $a = -i(\mathcal{Z} + \partial/\partial \mathcal{Z}^*)/\sqrt{2}$ and $a^\dagger = i(\mathcal{Z}^* - \partial/\partial \mathcal{Z})/\sqrt{2}$ such that the differential operators $D_x = \partial/\partial x + iy/2 = i(a + a^\dagger)/\sqrt{2}$ and $D_y = \partial/\partial y - ix/2 = i(a - a^\dagger)/\sqrt{2}$ can also be defined as well. With

these complex variables, it is easy to recover the kinetic energy operator $K = -(D_x^2 + D_y^2)$ to an effective number operator $2a^\dagger a + 1$ such that

$$\int \Psi^* K \Psi d\vec{r} = \frac{N(m+1)}{2} \left(\rho^2 + \frac{1}{\rho^2} + \alpha^2 \rho^2 \right) - mN + N|\mathcal{P}|^2. \quad (9)$$

Similarly, for the effective trapping potential operator, we have

$$\begin{aligned} \int \Psi^* V_{eff} \Psi d\vec{r} = & N (\omega_0^2 - 1) \left(\frac{m+1}{2} \rho^2 + |\mathcal{Z}_0|^2 \right) \\ & + N\lambda \left[\frac{1}{4}(m+2)(m+1)\rho^4 + |\mathcal{Z}_0|^4 + 2(m+1)\rho^2 |\mathcal{Z}_0|^2 \right]. \end{aligned} \quad (10)$$

Evaluating the angular momentum carried by the droplet,

$$\int \Psi^* L_z \Psi d\vec{r} = [i(\mathcal{P}^* \mathcal{Z}_0 - \mathcal{Z}_0^* \mathcal{P}) + m + 2|\mathcal{Z}_0|^2] N, \quad (11)$$

show three different mechanisms: the wavepacket repulsion dynamics, quantum phase imprinting and the rigid revolution. And, the interatomic energy term,

$$\int |\Psi|^4 \ln \left(\frac{|\Psi|^2}{\sqrt{e}} \right) d\vec{r} = \frac{N^2}{\pi(m!)^2 2^{2m+2}} \frac{1}{\rho^2} \left[(2m)! \ln \left(\frac{|C_m|^2}{4^m \sqrt{e}} \right) - \frac{(m+1)!}{2} \right. \quad (12)$$

$$\left. + m\Gamma'(2m+1) + (2m)(2m)! \ln \rho \right], \quad (13)$$

qualifies the self-bound feature through equilibrating the spatial attraction and repulsion. Eventually, the Lagrange function per atom is derived as

$$\begin{aligned} \mathfrak{L} = & -i(\mathcal{Z}^* \dot{\mathcal{Z}}_0 - \mathcal{Z} \dot{\mathcal{Z}}_0^*) - \frac{1}{2}(m+1)\dot{\alpha}\rho^2 + (\mathcal{P}^* \dot{\mathcal{Z}}_0 + \mathcal{P} \dot{\mathcal{Z}}_0^*) - \frac{m+1}{2} \left(\frac{1}{\rho^2} + \alpha^2 \rho^2 \right) \\ & - \omega_0^2 \left(\frac{m+1}{2} \rho^2 + |\mathcal{Z}_0|^2 \right) - \lambda \left[\frac{1}{4}(m+2)(m+1)\rho^4 + |\mathcal{Z}_0|^4 + 2(m+1)\rho^2 |\mathcal{Z}_0|^2 \right] \\ & - \frac{N}{\pi(m!)^2 2^{2m+2}} \frac{1}{\rho^2} \left[(2m)! \ln \left(\frac{|C_m|^2}{4^m \sqrt{e}} \right) - \frac{(m+1)!}{2} + m\Gamma'(2m+1) + (2m)(2m)! \ln \rho \right] \\ & + \Omega [i(\mathcal{P}^* \mathcal{Z}_0 - \mathcal{Z}_0^* \mathcal{P}) + m + 2|\mathcal{Z}_0|^2] - i(\mathcal{P}^* \dot{\mathcal{Z}}_0 - \mathcal{Z}_0^* \dot{\mathcal{P}}) - (|\mathcal{Z}_0|^2 + |\mathcal{P}|^2), \end{aligned} \quad (14)$$

through which the Euler-Lagrange equations and the equations of motion of the corresponding characteristic parameters can be obtained, i.e.,

$$\frac{d}{dt} \left(\frac{\partial L}{\partial \mathcal{P}^*} \right) - \frac{\partial L}{\partial \mathcal{P}^*} = 0 \quad \text{gives} \quad \dot{\mathcal{Z}}_0 = \mathcal{P} - i(\Omega - 1) \quad (15)$$

$$\begin{aligned} \frac{d}{dt} \left(\frac{\partial L}{\partial \dot{\mathcal{Z}}_0^*} \right) - \frac{\partial L}{\partial \dot{\mathcal{Z}}_0^*} = 0 \quad \text{gives} \quad \dot{\mathcal{P}} = & -2i\dot{\mathcal{Z}}_0 - (\omega_0^2 - 1) \mathcal{Z}_0 - 2\lambda |\mathcal{Z}_0|^2 \mathcal{Z}_0 \\ & - (\Omega - 1) \mathcal{P} + 2\mathcal{Z}_0 (\Omega - 1) - 2(m+1)\lambda \rho^2 \end{aligned} \quad (16)$$

$$\frac{d}{dt} \left(\frac{\partial L}{\partial \dot{\alpha}} \right) - \frac{\partial L}{\partial \dot{\alpha}} = 0 \quad \text{gives} \quad \dot{\rho} = \alpha \rho \quad (17)$$

$$\frac{d}{dt} \left(\frac{\partial L}{\partial \dot{\rho}} \right) - \frac{\partial L}{\partial \dot{\rho}} = 0 \quad \text{gives} \quad \dot{\alpha} = -\frac{1}{N(m+1)\rho} \frac{\partial E}{\partial \rho} \quad (18)$$

III. RESULTS AND DISCUSSION

Despite the fact that the 3D scattering lengths a^{3D} and $a_{\uparrow\downarrow}^{3D}$ provided by Refs. [12] and [34] can be chosen for suitably describing the liquid-like droplet regimes, it is a totally different scenario for 2D systems. To fit the simulation results of Ref. [31], the 2D scattering lengths a and $a_{\uparrow\downarrow}$ would take the form of $a = l_z \exp[-\sqrt{\pi/2} l_z / a^{3D}]$ and $a_{\uparrow\downarrow} = l_z \exp[-\sqrt{\pi/2} l_z / a_{\uparrow\downarrow}^{3D}]$, respectively, where $l_z = \sqrt{\hbar/2M\omega_z}$ is the oscillator length in the strong confinement direction.

To simulate a symmetric mixture of a quasi-2D ^{39}K self-bound oblate droplet [10], we choose $\omega_z = 2\pi \times 400 \text{ Hz}$, $a_{\uparrow\downarrow}^{3D} = -1800 a_0$, and $a^{3D} = 1100 a_0$ such that the weakly interacting regime is ensured by the inequality $1/\ln(a_{\uparrow\downarrow}/a) = 0.05 \ll 1$. In addition, by applying the Bogoliubov theory and the diffusion Monte Carlo simulation for $n_0 a^2 = 5 \times 10^{-10}$, the requirement of dilute liquids $na^2 \ll 1$ around the equilibrium density $n_0 = 2.5 \times 10^{14} \text{ m}^{-3}$ is also satisfied. As the chemical potential and the healing length can be approximately represented by $\mu \sim -n\hbar^2/M \ln^2(a_{\uparrow\downarrow}/a)$ and $\xi \sim \hbar/\sqrt{M|\mu|}$, respectively, and the latter represents the vortex core size of the rotating QD as well, they are approximately -0.412 and 2.2 at $n = 1.1n_0$ in the dimensionless scales. With these parameters, the particle number scale $\tilde{N} = n_0 l_z^2$ is about 81. For energy scale $\tilde{E} = \hbar\omega_z \sim 1.65 \text{ peV}$, the calculation of the ground state energy of this work shows that a rotating droplet of hundreds of atoms can be stably sustained in the extremely low temperatures of about tens of Kelvin, indicating that the time scale for tracing the droplet's dynamics before collapse approaches $\tau = 1/\omega_z = 0.4 \text{ ms}$.

A. Density Profile and Phase Portrait

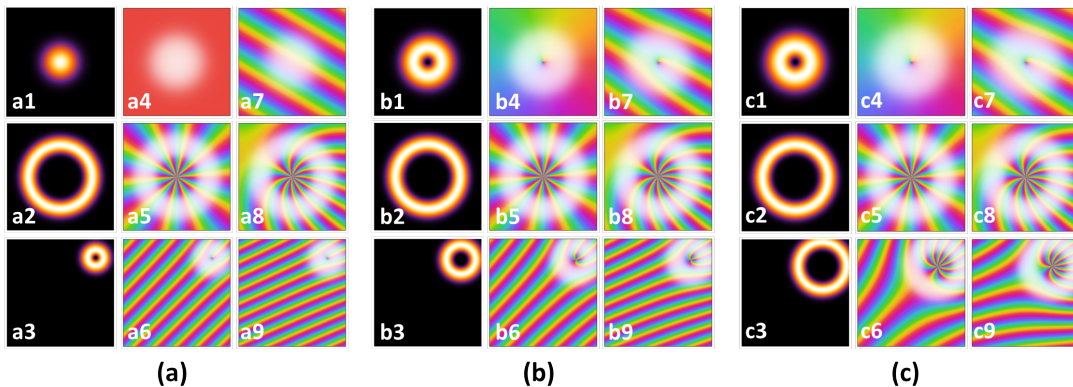


FIG. 1. (color online) Density profiles and phase portraits for (a) $N = 20$, (b) $N = 60$, and (c) $N = 100$, corresponding to $\Omega = 0.6, 1.4, 1.8$ (top to bottom) and initial momentum $p_x = 0, p_y = 0$ (middle), $p_x = 1.414, p_y = 2.449$ (right).

The influences of the confinement, nonlinear interaction, and rotational speed on the QD's configuration are first investigated. To investigate the stationary properties, the QD is claimed to be stirred adiabatically to ensure that equilibrium at certain Ω can be reached via the re-thermalization processes. However, to maintain bounded QDs at extremely high rotational speed, the emergence of strong attractions between squeezed atoms becomes inevitable in the fast expansion of the core size due to the very large orbital angular momentum (OAM) imposition on the vortex (VX) states. As a result, the QDs may teeter on the edge of collapse in the presence of the three-body collisions. To avoid this situation, we therefore suggest maximizing the total angular momentum of the VX state in energy minimization. Along with the lowest Landau level approximation, the exploitation of this constraint is thus useful to estimate the upper bound of the topological charge and the deflection distance given by $m_{max} = (\Omega - \epsilon/2 - 1)/\lambda - 1$ and $R = 2\sqrt{\Omega - \epsilon/2 - 1 - (m + 1)\lambda\rho^2}/\sqrt{\lambda}$, respectively. With this restriction, the limiting fraction of the cross-sectional area occupied by the vortex cores estimated in the Thomas-Fermi regime for dilute atomic gases [35] can also be validly applied for QDs.

Figure 1 shows the density profiles and phase portraits for (a) $N = 20$, (b) $N = 60$, and (c) $N = 100$, corresponding to $\Omega = 0.6, 1.4, 1.8$ (top to bottom) and initial momentum $p_x = 0, p_y = 0$ (middle), $p_x = 1.414, p_y = 2.449$ (right). At slow rotations, it is found that when the particle number is low, the CM state with $m = 0$ and $R = 0$ is the energetically favorable ground state, even when Ω is slightly larger than one, as shown in Fig. 1(a1). When the particle number increases, the repulsive LHY terms play the decisive role in the formation of the VX states with nonzero m , such as the doughnuts shown in Figs. 1(b1) and (c1) that both have $m = 1$. As we increase the rotational speed to $\Omega = 1.4$, Figs. 1(a2), (b2), and (c2) show the possibility of the formation of giant vortices with $m \geq 10$ and large cores due to strong centrifugal forces. On the other hand, at even faster rotations with $\Omega = 1.8$, the system prefers to form off-center vortex (OCVX) states with nonzero R instead, such as shown in Figs. 1(a3), (b3), and (c3). For these deflected QDs, the cores of the vortices enlarge with the increase in the particle number, but are lower than those of the aforementioned VX states. Within weakly nonlinear interactions, this phenomenon can be attributed to the counterbalance between the centrifugal force and the strong compression provided by the anharmonic potential.

In the middle and right columns, the color lines depict the spatial phase distribution in the cases $\vec{p}(0) = 0$ and $\vec{p}(0) \neq 0$. For the CM state, the phase portraits in (a4) and (a7) display the wavefronts of plane waves, whereas for VX states the radial patterns in (b4), (c4), (a5), (b5), and (c5) imply the repetition rate of phase variation in 2π , which just equals the corresponding topological charge number. However, the launch of a finite initial momentum produces strain on the surface of the QD, thus imprinting an additional phase upon its wavefunction and skewing the radial wavefronts, such as shown in (b7), (c7), (a8), (b8), and (c8). For the OCVX states, the emergence of the fork-like phase distributions, presented in (b6), (b9), (c6), and (c9), due to the displacement of the ring center is the reveal of the spiral phase from the grating diffraction as observed in the optical vortices, such as shown in Fig. 2. Both QDs and optical vortices share a number of key features. In the paraxial approximation, the solution of the Helmholtz equation of a cylindrical symmetric optical vortex is the Laguerre-Gaussian function,

$$LG_{p\ell}(r, \phi, z) = \sqrt{\frac{2p!}{\pi(p+|\ell|)!} \frac{1}{w(z)}} \left[\frac{\sqrt{2}r}{w(z)} \right]^{| \ell |} \exp \left[\frac{-r^2}{w^2(z)} \right] L_p^{|\ell|} \left(\frac{2r^2}{w^2(z)} \right) \exp[i\ell\phi] \exp \left[\frac{ik_0 r^2 z}{2(z^2 + z_R^2)} \right] \exp \left[-i(2p + |\ell| + 1) \tan^{-1} \left(\frac{z}{z_R} \right) \right], \quad (19)$$

where $w(z) = w_0 \sqrt{1 + (z/z_R)^2}$ is the beam width with w_0 being the beam waist, z_R the Rayleigh range, and $(2p + |\ell| + 1) \tan^{-1} (z/z_R)$ the Gouy phase corresponding to the angular index ℓ and the radial index p . With the implementation of the spatial light modulator (SLM), we can easily generate high-order optical vortices and access their phase information. As demonstrated in Fig. 2(a), the density profile of the LG_{010} mode with intensity singularity is the first-order diffraction at the focal length, whereas the phase singularities in (b) and (c) are revealed by the interference of the LG_{010} mode with a Gaussian spherical wave and a Gaussian plane wave, respectively. Since many of the similarities between the simulation and the experimental results of the two systems can be addressed, the optical vortex can be thought of as the classical correspondence of the rotating QD. The emergence of the intensity and phase singularities in rotating QDs provide evidence of the controllable generation of nonzero OAM upon atoms, and further the possibility of synthesizing orbital magnetism in quantum liquids. Therefore, as Figs. 1(a3), (a6), and (a9) show, when the particle number is not high enough to stably support the formation of a multiple charged vortex, the rotation induced phase singularity in the tiny vortex core could be diminished as the translational effect is involved, resulting in the hindering of the persistent current generation and destruction of the superfluidity. This feature, which can be verified later in the phase diagram, thus suggests a critical particle number N_c for the formation of a stable QD vortex in the weakly interacting and dilute liquids, below which there can be no extrinsic magnetic dipole moment nor observation of paramagnetism.

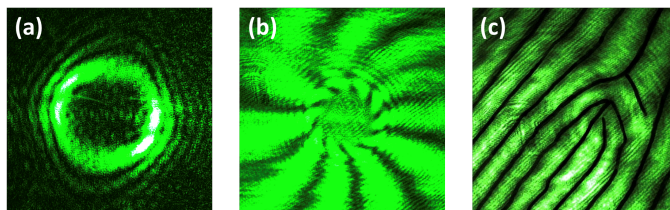


FIG. 2. (color online) (a) Generation of the optical vortex of LG_{010} mode with intensity singularity using SLM. The phase singularities can be observed from the interference of the LG_{010} mode with (b) a Gaussian spherical wave and (c) a Gaussian plane wave

B. Phase Diagram

Figure 3(a) shows the $N - \Omega$ phase diagram of the system's ground state with the inclusion of the maximum circulation restriction, in which (i) to (iv) depict the regions for CM, VX, OCVX, and off-center-of-mass (OCM) states, respectively. In Fig. 3(b), the blue and red curves show the expectation value of single-particle's OAM $\langle L_z \rangle = m + 2|Z_0|^2$ as a function of Ω with and without following the restriction of maximum circulation that can be distinguished from the appearance of an extended plateau. The inset also shows the energy variation as a function of Ω for the $m = 0$ CM state and $m = 1, 3, \dots, 11$ VX states. With the increase of Ω , the phase transition from the CM state to the VX state with large multiple singularities and lower energies occurs to maintain the QD's stability. Across the boundary of (ii) and (iii), the phase transition from the VX state to the OCVX state occurs. The QDs attempt

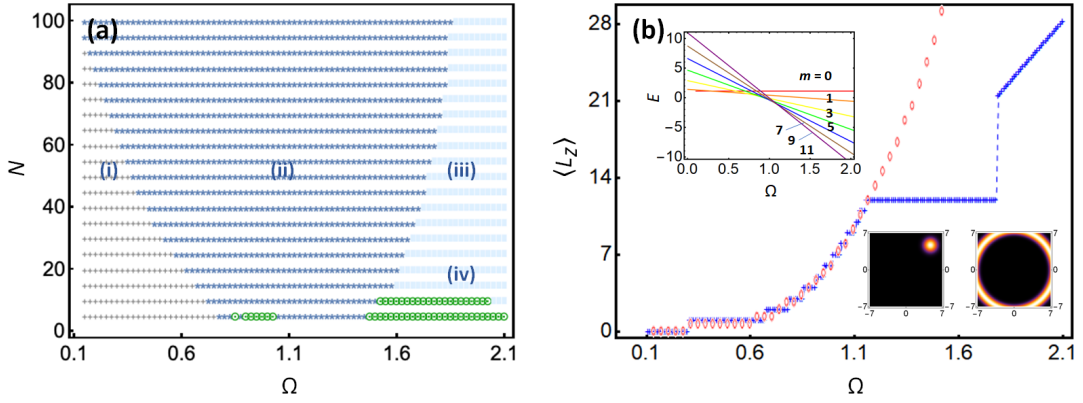


FIG. 3. (color online) (a) The $N - \Omega$ phase diagram, in which (i) to (iv) depict the regions for CM, VX, OCVX, and OCM states, respectively. For $N = 60$, the blue and red curves in (b) show the expectation value of the OAM $\langle L_z \rangle$ as a function of Ω with and without following the restriction of maximum circulation. At $\Omega = 1.8$, the density profile of the VX state with a huge core reveals a metastable contrast of a stable OCM state formed in the few particle regimes. The inset shows the energy variation as a function of Ω for the $m = 0$ CM state and $m = 1, 3, \dots, 11$ VX states.

to keep stable at extremely high rotational speed Ω by abruptly lowering their rotational inertia concerning the CM of the atoms via shrinking the vortex core size but raising the rotational kinetic energy via configuring themselves to off-axis vortices. Otherwise, the formation of VX states with huge cores far beyond the theoretical limit and squeezed atomic distribution, such as the density profile shown in Fig. 3(b), where $\Omega = 1.8$, would effectively bear an inter-attractive interaction, and thus is only metastable and fragile against three-body collisions. As a comparison, stable OCM states can be formed in the few particle and fast rotation regimes (iv). However, when the particle number is low, the QDs of ultra-dilute liquids can be stably sustained if they are energetically more favorable than the atomic cloud subjected to an effective 2D MF interaction given by

$$V^{2D}(\vec{r}) = \frac{\sqrt{8\pi}\hbar^2 a_s}{ml_z} \delta^{2D}(\vec{r}). \quad (20)$$

The presence of OCM states near $\Omega = 1$ in Fig. 2(a) is the signature of the dynamic instability that the gas-liquid phase transition can be induced due to particle fluctuations.

It should be noticed that for certain N and Ω , the stability condition

$$\frac{\partial^2 E}{\partial \rho^2} \frac{\partial^2 E}{\partial R^2} - \left(\frac{\partial^2 E}{\partial \rho \partial R} \right)^2 > 0 \quad (21)$$

must be satisfied when determining the QD's ground state. Therefore, while the CM states in the region (i) are found to violate the inequality, the system would try to maintain its stability by removing the atoms from the dense peak to pinning on the trap center, resulting in the creation of the embedded vortex with multiple circulations when initiating a rotation. Although it was reported that the multiple singly quantized vortex clusters can be created in the QDs at slow rotations [36], they are metastable and cause the deformation of the QDs.

C. Periodicity and Stability

We can trace QD's dynamics by solving multiple coupled equations of motion given by the Euler-Lagrange equation

$$\frac{d}{dt} \left(\frac{\partial L}{\partial \dot{q}} \right) - \left(\frac{\partial L}{\partial q} \right) = 0 \quad (22)$$

for the characteristic parameters $q = \rho, \alpha, \vec{R}$, and \vec{P} . Because of the lack of rotational kinetic energy, the perturbed CM state shows its instability in the short-term evolution and eventually crashes when it escapes from the trap confinement (Fig. 4(a)). With the increase in rotational speed, the dominant VX state shows its stability by adjusting itself to the lowest-Landau level (Fig. 4(b)). At rapid rotations, Fig. 4(c) shows that OCVX maintains stability by lowering the OAM but shrinking itself to steadily precess against the perturbation.

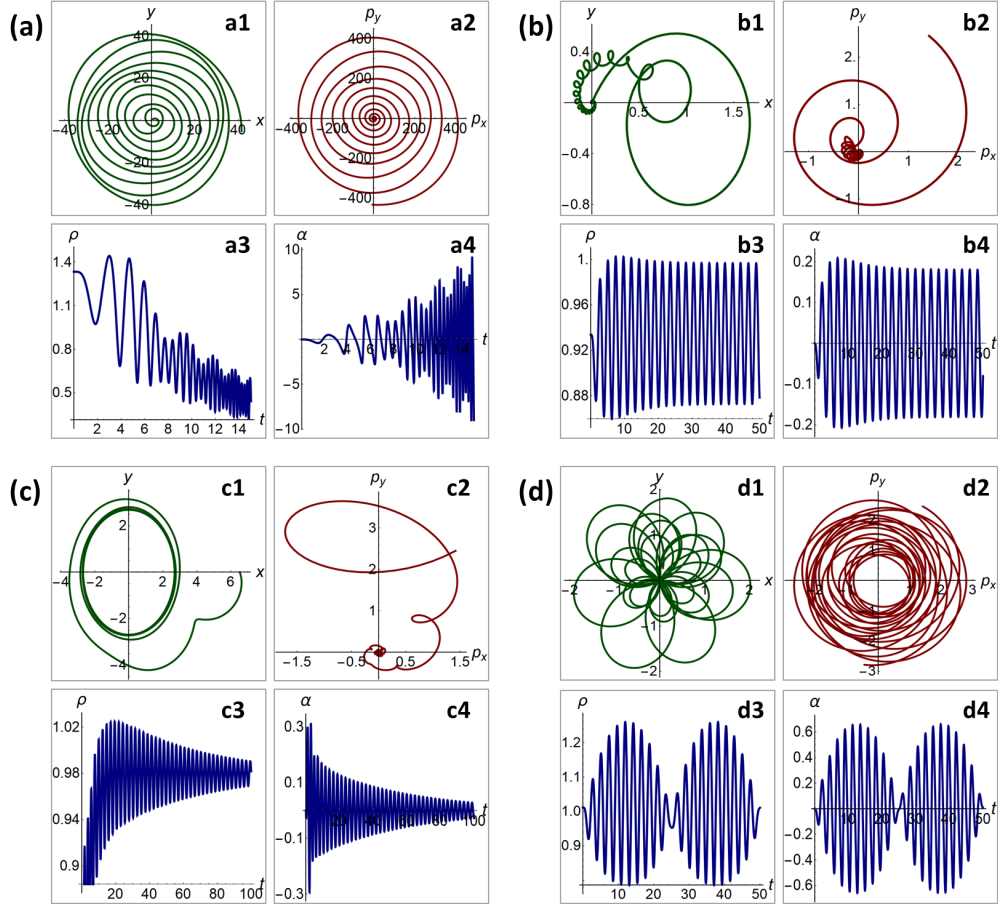


FIG. 4. (color online) Trajectory \vec{R} and \vec{P} , width ρ , and conjugate curvature coefficient α for (a)-(c) $N = 20$ and $\Omega = 0.6, 1.4$, and 1.8 , (d) $N = 100$ and $\Omega = 1.0$.

At $\Omega = 1.0$, the externally-applied effective centripetal force for an orbital motion vanishes, leaving a nonzero Coriolis force induced by the velocity variation in the zonal direction that launches a self-curing rotational motion for the QD. As shown in Fig. 4(d), the quasi-periodic trajectories and breathings provide evidence of the emergence of the collective excitation of the surface mode in the VX state. In the presence of the anharmonic trapping and the nonlinear effects, the orbit of the QD does not strictly close upon itself after a finite number of oscillations, and neither does it open. Instead, as the lobes reveal, the evolution of the QD shows a multiple-periodic motion between the turning points. Similar to that for a periodic motion driven by the central-force field, the area enclosed by the moving trajectory is still a rational fraction $2\pi(a/b)$ —after b periods, the radius of the vector of the QD will have made a complete revolutions and will have returned to its original position.

For strongly interacting cases, the vortices are much smaller than the system size and the radius of curvature of the density profile. The results of homogeneous systems then apply to support the formation of vortex arrays. As a result, for a fixed angular momentum, the wave functions are written as the sum of noninteracting particle states of different angular momenta rather than the ansatz as Eq. (4) presents. On the other hand, in the region containing multiple quantized vortices, the vortex cores are large and the vortex density is suppressed such that the individual vortices become indiscernible. Accordingly, although the multiple quantized vortices carrying high topological charges are not thermodynamically stable and energetically favorable in the homogeneous superfluids or harmonic-confined systems, the periodicity and stability analyses in this work demonstrate that the vortex configurations in anharmonically-trapped rotating QDs can be stably supported.

D. Persistent Currents

Rotation at angular velocity Ω can be regarded as a perturbation to the nonrotating system Hamiltonian:

$$-\vec{\Omega} \cdot \vec{L} = -m \sum_{\mathbf{q}} \vec{j}_{\mathbf{q}}^{\dagger} \cdot \vec{A}_{\mathbf{q}}, \quad (23)$$

where $\vec{j}_{\mathbf{q}}^{\dagger}$ is the particle current density fluctuation and $\vec{A}_{\mathbf{q}}$ is the Fourier transform of the transverse artificial vector potential. With the application of linear response theory, this fluctuation will give rise to the mass current in the condensate frame. For low-energy scattering around $\mathbf{q} = 0$, the current density in the coordinate representation can be described in terms of the condensate wavefunction,

$$\vec{j} = \frac{\hbar}{2Mi} \left[\psi^*(\vec{r}) \vec{\nabla} \psi(\vec{r}) - \psi(\vec{r}) \vec{\nabla} \psi^*(\vec{r}) \right], \quad (24)$$

the substitution of a general order parameter $\psi(\vec{r}) = f(\vec{r})e^{i\phi(\vec{r})}$ in Eq. (24) gives $\vec{j} = (\hbar/M)\vec{\nabla}\phi(\vec{r})|\psi(\vec{r})|^2$, which implies that motion of the condensate governed by velocity field $\vec{v}(\vec{r}) = (\hbar/M)\vec{\nabla}\phi(\vec{r})$ is a potential flow and is irrotational unless there exist some singularities in the local phase $\phi(\vec{r})$. As previously mentioned, the VX and OCVX states that carry nonzero OAM are similar to the optical vortices of Laguerre-Gaussian modes with phase singularity and intensity singularity in the optical field. Moreover, while the quantum number m of the topological charge is found equal to the electromagnetic field angular momentum flux density per photon with respect to the transverse position, the circulation in the vortex beams is specified to be fluid-like. In analogy with the photon beams, the emergence of embedded singularities in the neutral atoms thus provide the opportunity to examine the coherence property and the superfluidity that are associated with the two-body reduced density matrix via investigating the persistent current (PC) generation in the QDs.

Described by the wave function of Eq. (5), the dimensionless total current density of the QD consists of four parts:

$$\vec{j} = g_m(\vec{r}, \vec{R}) \left[4m(\vec{r} - \vec{R})^{-2} [-(y - Y_0)\hat{x} + (x - X_0)\hat{y}] + [\alpha(x - X_0) + p_x - Y_0]\hat{x} + [-\alpha(y - Y_0) - p_y + X_0]\hat{y} \right], \quad (25)$$

in which $g_m(\vec{r}, \vec{R}) = 4^{-m} C_m^2 (\vec{r} - \vec{R})^{2m} \exp[-(\vec{r} - \vec{R})^2/2\rho^2]$. As expected, Eq. (25) reveals that the generation of PCs can only be observed in the quantum states specified with nonzero circulation. The phase shifts due to the MF expansion and the relative repulsion of the wavepacket have no contributions to the generation of the PCs, but would alter the flow of the ordinary fluids. In Fig. 5 we demonstrate the snapshots of the persistent density distribution at $t = 0$ for $N = 100$ and (a) $\Omega = 0.6$, (b) $\Omega = 1.4$, and (c) $\Omega = 1.8$. For each column, the upper panel corresponds to $\vec{p}(0) = 0$, and the lower one corresponds to $\vec{p}(0) \neq 0$. At slow rotating speed, the directional swirling of the dense atomic flow is a result of the Coriolis force effect. In experiments of vortex creation for the two-component dilute BEC gases, where the self-interaction of one component is different from the other, the Hamiltonian is assumed to be invariant under simultaneous rotation of all the hyperfine states. In that work, the generation of annual PCs is attributed to lacking the common kind of topological stability as a single-component system such as He-4. The reasoning, however, will not be applied to generating asymmetric PCs in this work, since the scattering strength imbalance among different species has already been considered in the effective LHY nonlinear interaction, and therefore there is no spin current generation in this work. The nonuniform distribution of the PCs of multiple topological charges is mainly attributed to the supposition of the gauge-induced azimuthal and linear flows, and at $t > 0$, the nonhomogeneity can be enhanced or reduced according to the wavepacket breathing. Together with the nonlinear-modulated self-bound effect, the PC is established as a partially coherent flow with mixed ideal and rigid-like fluids. As a result, the imbalance in vorticity will produce a shear force in the atomic cloud, providing strong support for driving the complex revolutions demonstrated in Fig. 4.

IV. CONCLUSION

This work investigated the dynamics of trapped rotating QDs with nonlinear LHY interaction. The stationary properties were studied using the variational method by minimizing energy functional based on Laughlin-like wavefunction with LLM. We explored the density profile, phase portrait, and phase diagram of the CM state, VX state, OCVX state, and OCM state. We also analyzed the periodicity and stability of QD's breathing and trajectory. The rotating QD can be thought of as the quantum correspondence of the optical vortex. The emergence of the intensity and phase singularities in rotating QDs provide evidence of the controllable generation of nonzero OAM upon atoms, and the possibility of synthesizing orbital magnetism in quantum liquids. With the increase in the rotational speed,

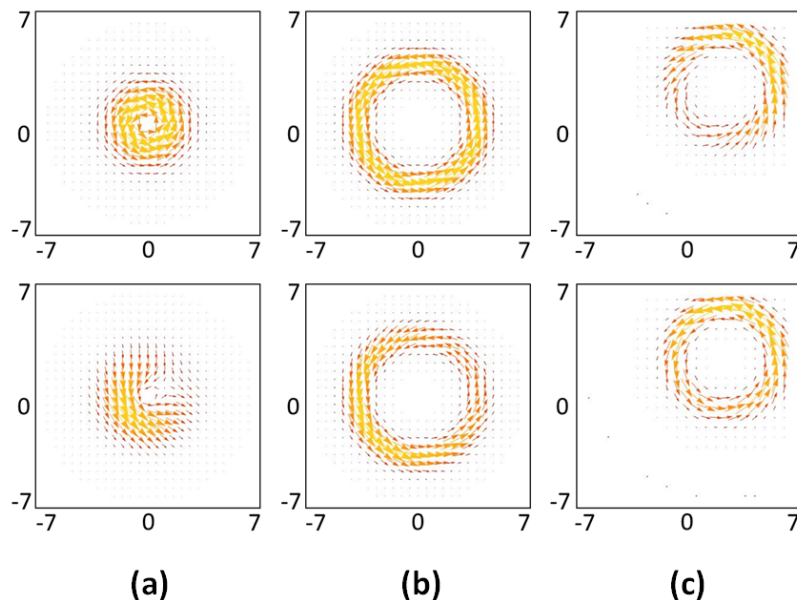


FIG. 5. (color online) Persistent current density distribution for $N = 100$ and (a) $\Omega = 0.6$, (b) $\Omega = 1.4$, and (c) $\Omega = 1.8$. For each column, the upper panel corresponds to $\tilde{p}(0) = 0$, and the lower one corresponds to $\tilde{p}(0) \neq 0$.

the VX states tend to occupy the lowest-Landau level to maintain their stability, which is consistent with the QH phenomenon. At rapid rotations, the OCVX state with lower m and smaller core size becomes energetically favorable by showing the possibility to steadily precess against the perturbation. At $\Omega = 1.0$, the externally-applied effective centripetal force for an orbital motion vanishes, leaving a nonzero Coriolis force induced by the velocity variation in the zonal direction that launches a self-curing rotational motion for the QD. The quasi-periodic trajectories and breathings provide evidence for the emergence of the collective excitation of the surface mode in the VX state. As a signature of superfluids, the generation of nonuniform PCs of multiple topological charges is attributed to the supposition of the gauge-induced azimuthal and linear flows and reveals the effect of nonlinear modulation. Instead of forming metastable vortex lattices, our work verifies that QDs with multiple topological charges can be stably supported in the anharmonically confined rapid rotating system.

V. ACKNOWLEDGEMENT

We thank the Ministry of Science and Technology, Taiwan for partial financial support under grants MOST 110-2221-E-845-004 and MOST 111-2112-M-034-001.

-
- [1] M. H. Anderson, J. R. Ensher, M. R. Matthews, C. E. Wieman, and E. A. Cornell, *Science* **269**, 198 (1995).
 - [2] C. C. Bradley, C. A. Sackett, J. J. Tollett, and R. G. Hulet, *Phys. Rev. Lett.* **75**, 1687 (1995).
 - [3] K. B. Davis, M.-O. Mewes, M. R. Andrews, N. J. van Druten, D. S. Durfee, D. M. Kurn, and W. Ketterle, *Phys. Rev. Lett.* **75**, 3969 (1995).
 - [4] C. A. Regal, M. Greiner, and D. S. Jin, *Phys. Rev. Lett.* **92**, 040403 (2004).
 - [5] M. W. Zwierlein, C. A. Stan, C. H. Schunck, S. M. F. Raupach, A. J. Kerman, and W. Ketterle, *Phys. Rev. Lett.* **92**, 120403 (2004).
 - [6] G. B. Partridge, K. E. Strecker, R. I. Kamar, M. W. Jack, and R. G. Hulet, *Phys. Rev. Lett.* **95**, 020404 (2005).
 - [7] D. M. Eagles, *Phys. Rev.* **186**, 456 (1969).
 - [8] T. Köhler, K. Góral, and P. S. Julienne *Rev. Mod. Phys.* **78**, 1311 (2006).
 - [9] T. D. Lee, K. Huang, and C. N. Yang, *Phys. Rev.* **116**, 1135 (1957).
 - [10] C. R. Cabrera, L. Tanzi, J. Sanz, B. Naylor, P. Thomas, P. Cheiney, and L. Tarruell, *Science* **359**, 301 (2018).
 - [11] P. Cheiney, C. R. Cabrera, J. Sanz, B. Naylor, L. Tanzi, and L. Tarruell, *Phys. Rev. Lett.* **120**, 135301 (2018).

- [12] G. Semeghini, G. Ferioli, L. Masi, C. Mazzinghi, L. Wolswijk, F. Minardi, M. Modugno, G. Modugno, M. Inguscio, and M. Fattori, *Phys. Rev. Lett.* **120**, 235301 (2018).
- [13] I. Ferrier-Barbut, H. Kadau, M. Schmitt, M. Wenzel, and T. Pfau *Phys. Rev. Lett.* **116**, 215301 (2016).
- [14] M. Schmitt, M. Wenzel, F. Böttcher, I. Ferrier-Barbut, and T. Pfau, *Nature* **539**, 259 (2016).
- [15] I. Ferrier-Barbut, M. Wenzel, F. Böttcher, T. Langen, M. Isoard, S. Stringari, and T. Pfau, *Phys. Rev. Lett.* **120**, 160402 (2018).
- [16] L. Chomaz, S. Baier, D. Petter, M. J. Mark, F. Wächtler, L. Santos, and F. Ferlaino, *Phys. Rev. X* **6**, 041039 (2016).
- [17] D. S. Petrov, *Phys. Rev. Lett.* **115**, 155302 (2015).
- [18] Z. H. Luo, W. Pang, Y. Y. Li, and B. A. Malomed, *Front. Phys.* **16**, 32201 (2021).
- [19] M. R. Matthews, B. P. Anderson, P. C. Haljan, D. S. Hall, C. E. Wieman, and E. A. Cornell, *Phys. Rev. Lett.* **83**, 2498 (1999).
- [20] K. W. Madison, F. Chevy, W. Wohlleben, and J. Dalibard, *Phys. Rev. Lett.* **84**, 806 (2000).
- [21] B. P. Anderson, P. C. Haljan, C. A. Regal, D. L. Feder, L. A. Collins, C. W. Clark, and E. A. Cornell, *Phys. Rev. Lett.* **86**, 2926 (2001).
- [22] Z. Dutton, M. Budde, C. Slowe, and L. V. Hau, *Science* **293**, 663 (2001).
- [23] K. W. Madison, F. Chevy, V. Bretin, and J. Dalibard, *Phys. Rev. Lett.* **86**, 4443 (2001).
- [24] J. R. Abo-Shaer, C. Raman, J.M. Vogels, and W. Ketterle, *Science* **292**, 476 (2001).
- [25] E. Lundh, Multiply quantized vortices in trapped Bose-Einstein condensates, *Phys. Rev. A* **65**, 043604 (2002).
- [26] P. Engels, I. Coddington, P. C. Haljan, V. Schweikhard, and E. A. Cornell, *Phys. Rev. Lett.* **90**, 170405 (2003).
- [27] B. A. Malomed, *Physica D* **399**, 108 (2019).
- [28] Y. Y. Li, Z. P. Chen, Z. H. Luo, C. Q. Huang, H. S. Tan, W. Pang, and B. A. Malomed, *Phys. Rev. A* **98**, 063602 (2018).
- [29] Y. V. Kartashov, B. A. Malomed, L. Tarruell, and L. Torner, *Phys. Rev. A* **98**, 013612 (2018).
- [30] X. L. Zhang, X. X. Xu, Y. Y. Zheng, Z. P. Chen, B. Liu, C. Q. Huang, B. A. Malomed, and Y. Y. Li, *Phys. Rev. Lett.* **123**, 133901 (2019).
- [31] D. S. Petrov and G. E. Astrakharchik, *Phys. Rev. Lett.* **117**, 100401 (2016).
- [32] T. Ilg, J. Kumlin, L. Santos, D. S. Petrov, and H. P. Büchler, *Phys. Rev. A* **98**, 051604(R) (2018).
- [33] V. N. Popov, *Theor. Math. Phys.* **11**, 565 (1972).
- [34] T. G. Skov, M. G. Skou, N. B. Jørgensen, and J. J. Arlt, *Phys. Rev. Lett.* **126**, 230404 (2021).
- [35] U. R. Fischer and G. Baym, *Phys. Rev. Lett.* **90**, 140402 (2003).
- [36] M. N. Tengstrand, P. Stürmer, E. Ö. Karabule, and S. M. Reimann, *Phys. Rev. Lett.* **123**, 160405 (2019).